Steel and Composite Structures, *Vol. 34, No. 2 (2020) 171-188*
DOI: https://doi.org/10.12989/scs.2020.34.2.171

Flexural Strength of cold-formed steel built-up composite beams with rectangular compression flanges

M. Adil Dar[1], N. Subramanian[2], Dawood A. Dar[3], A.R. Dar*[3],
M. Anbarasu[4], James B. P. Lim[5] and Soroush Mahjoubi[6]

[1]Department of Civil Engineering, Indian Institute of Technology Delhi, New Delhi, India
[2]Consulting Engineer, Maryland, USA
[3]Department of Civil Engineering, National Institute of Technology Srinagar, J&K, India
[4]Department of Civil Engineering, Government College of Engineering Salem, Tamilnadu, India
[5]Department of Civil & Environmental Engineering, University of Auckland, New Zealand
[6]School of Civil Engineering, Iran University of Science and Technology, Narmak, Tehran, Iran

(*Received August 31, 2019, Revised November 15, 2019, Accepted December 1, 2019*)

Abstract. The past research on cold-formed steel (CFS) flexural members have proved that rectangular hollow flanged sections perform better than conventional I-sections due to their higher torsional rigidity over the later ones. However, CFS members are vulnerable to local buckling, substantially due to their thin-walled features. The use of packing, such as firmly connected timber planks, to the flanges of conventional CFS lipped I-sections can drastically improve their flexural performance as well as structural efficiency. Whilst several CFS composites have been developed so far, only limited packing materials have been tried. This paper presents a series of tests carried out on different rectangular hollow compression flanged sections with innovative packing materials. Four-point flexural tests were carried out to assess the flexural capacity, failure modes and deformed shapes of the CFS composite beam specimens. The geometric imperfections were measured and reported. The North American Specifications and Indian Standard for cold-formed steel structures were used to compare the design strengths of the experimental specimen. The test results indicate clearly that CFS rectangular 'compression' flanged composite beams perform significantly better than the conventional rectangular hollow flanged CFS sections.

Keywords: cold-formed steel; composite sections; experiment; flexural members; local buckling

1. Introduction

Cold-formed steel (CFS) members have a wide range of applications as structural members, primarily due to their numerous advantages like simpler fabrication, high strength-to-weight ratio, etc. CFS sections have a high width-to-thickness ratio, thus making them vulnerable to local buckling under compressive stresses. In the past decade, significant developments have been made in the design of CFS members for better suitability with respect to civil engineering utilities (Usefi *et al*. 2019, Muftah *et al.* 2019, Sani *et al*, 2019, 2018, Sharafi *et al*. 2018, Javed *et al*. 2017, Hancock 2016, Sani *et al*. 2016, Biggs *et al*. 2015, Kim *et al.* 2015, ValseIpe *et al.* 2012, Yang and Lui 2012). CFS flexural members possess inelastic reserve strengths at their ultimate stage and can be mobilized substantially (Kumar and Sahoo 2016). Well-designed CFS sectional profiles and efficient stiffening arrangements have the potential to either delay or completely eliminate the instability failures, thus permitting the cross-section to reach its ultimate capacity (Dar *et al.* 2015a). Partial stiffening of buckling vulnerable zones in CFS beams can substantially improve their flexural performance (Dar et.al. 2019a). Early local buckling wave formation in CFS built-up members with a large flat-to-width ratio does not restrict the member's capacity to resist further loads (Dar *et al*. 2018a). Corrugated profiling of CFS sheets imparts substantial in-plane rigidity to such profiles under concentric loading (Priyanga and Ramalingam 2018). Under compressive loading, the variation in web thickness of built-up CFS sections influences the strength and deformation behavior more than that of in flanges (Khate *et al.* 2018). The past two decades witnessed the development of a new structural system i.e., steel beams with corrugated web that affords a significant weight reduction of these beams, compared with hot-rolled or welded ones. Global imperfections significantly influence the efficiency of the strengthening measures adopted for CFS beams (Dar *et al.* 2019b). External angle stiffening of CFS I-beams improve their strength as well as stiffness response significantly (Dar *et al.* 2019c)

Hollow tubular flange plate girders possess larger flexural and shear capacities over the standard I-section plate girders (Hassanein 2015). A novel CFS section i.e., riveted rectangular hollow flanged channel beam (RHFCB) has two torsionally rigid rectangular hollow flanges, attached to the web through intermittent rivet fastening. The absence of free edges in RHFCB prevents local buckling,

*Corresponding author, Professor
E-mail: abdulrashid@nitsri.net

http://www.techno-press.org/?journal=scs&subpage=6 ISSN: 1229-9367 (Print), 1598-6233 (Online)

thus improves its structural performance. The moment capacity of these novel sections reduces with the increase in rivet spacing (Siahaan *et al.* 2018). This improvement was primarily observed due to the reduction in the half-wave buckling length between the screws, along the length of the beam. Ye *et al*. (2016) fabricated efficient CFS sections for flexure, with an objective to maximize their flexural performance. This was primarily carried out by increasing the number of folds for further stiffening the cross-section to achieve the same. Optimization of CFS sections can improve the load-carrying capacity, leading to economical structural systems. The new folded-flanged sections provide better flexural strength than the standard CFS sections with the same amount of material. Magnucka-Blandzi (2010) performed an extensive analytical study on the efficient shaping of CFS channel beams with double-box flanges under pure flexure. These beam sections showed better resistance towards buckling compared to conventional lipped channel beams.

Hassanein *et al*. (2017) conducted tests on cementitious material-filled square thin-walled steel flexural members. The confined concrete as a filler material in the hollow regions resisted the buckling of the plate elements of the cross-section that helped in enhancing the flexural resistance of these sections. Gao *et al.* (2014) performed tests on pentagonal flanged beams filled with concrete. The capacity of these beams with transverse stiffeners at mid-span was nearly twice as that of beams without stiffeners. The beams without transverse stiffeners failed by lateral distortional and local buckling of the web while the ones with transverse stiffeners failed by lateral torsional buckling.

Awaludin *et al*. (2015) developed CFS-timber composite compression members for roof structures with less maintenance against termites. The composite sections comprising of 15mm thick timber sheets attached to the web of CFS sections with screwed connections proved significantly better in terms of strength and stiffness when compared to the non-composite members. The failure modes included a combination of local buckling and flexural-torsional buckling. Li *et al*. (2014) carried out an experimental study on the flexural capacity of I-section bamboo-steel composite beams. The results indicated that the bamboo plywood and CFS channel can form a well-integrated composite cross-section. The performance of this CFS composite cross-section is affected by the thickness of both the bamboo plywood and steel channel. Dar *et al.* (2018b) conducted an experimental study on the structural performance evaluation of CFS composite beams by testing them with simply supported end conditions and under four-point loading. In the first trial, a low-cost innovative stiffening arrangement (using high density expanded polystyrene as packing) to fill the hollow space within the proposed innovative box compression flange was used. However, such a stiffening arrangement could not prevent the local buckling failure of the top face of box compression flange at a lower load and hence was not recommended. The replacement of softer expanded polystyrene by wooden pads at load application points resulted in drastic improvement in the load-carrying capacity. The use of firmly connected timber planks throughout the compression flange drastically improved the load-carrying capacity further.

CFS members are prone to local buckling instabilities under lower compressive stresses. These local buckling instabilities take place well before the material reaches its yield strength. This leaves the section under-utilized compared to its ultimate capacity which is governed by strength failure. The inelastic reserve strength at the ultimate stage under flexural loading is a major advantage of CFS sections. The primary aim of this study was to develop novel CFS composite sections, possessing higher strength and stiffness, with improved local buckling resistance in order to utilize their maximum sectional capacities. The past research on the same where concrete has been used as a filler material defeats the light-weighted constructional feature of CFS construction. Furthermore, only limited research has been carried out on other lightweight packing materials. Thus, leaving a major scope for adopting other judiciously selected lightweight packing materials for the same, a part of which has been addressed in the current research work. This paper presents a series of tests carried out on different rectangular hollow compression flanged sections with innovative packing materials. Four-point flexural tests were carried out to assess the flexural capacity, failure modes and deformed shapes of the CFS composite beam specimens. The geometric imperfections were measured and reported. The North American Specifications and Indian Standards for cold-formed steel structures were used to compare the design strengths of experimental specimens.

2. Test specimens

The basic reason behind the adoption of a rectangular hollow flange profile was to attain better torsional stability, unlike the conventional I-section formed by connecting two-lipped CFS channels in a back-to-back configuration. Since, after the flange, some part of the compressive stress (which is decreases as we move towards the neutral axis) is resisted by the web as well, adopting a hollow web would further improve the flexural performance of these sections. This paved the way for having adopted the two CFS profiles, as shown in Figs. 1 (a) and 1(b). Seven specimens were fabricated using different packing materials in two CFS profiles as shown in Figs. 1 (a) and 1(b). Profile A has a rectangular compression flange, while profile B has both rectangular compression flange as well as the web as shown in Figs. 1 (a) and 1(b).. Shearing machine was used to cut the sheets into their requisite sizes. Hydraulic press brake was used for profiling the cut sheets obtained from the shearing machine. Once all the components were prepared in their required sizes, the channels were first clamped together along with the packing (if any) in-between and then firmly connected together using hexagon head self-drilling screw fasteners (6.4 mm in diameter and 35 mm in length), as shown in Fig. 1(c). The screws were placed at nearly the middle third points along the depth of the web at a uniform longitudinal spacing of 200 mm as shown in

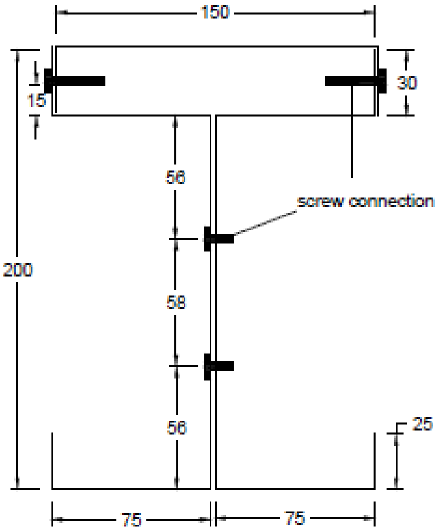

(a) Profile A

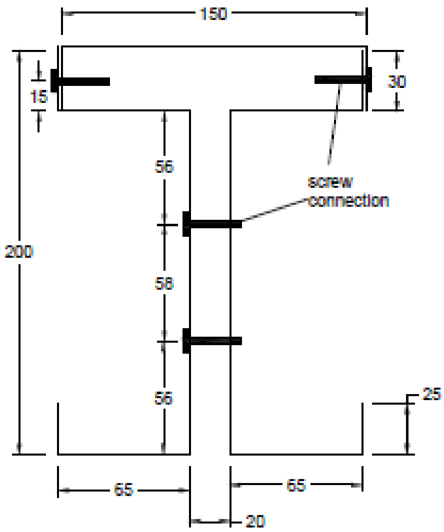

(b) Profile B


(c) Self drilling screw used

Fig. 1 CFS cross-sectional profiles adopted for preparation of specimens

Fig. 2 Overall view of the test specimens before testing

profiles-A and B. The top plate of the rectangular compression flange was then placed along with the packing (if any) and clamped with the channel assembly types of light-weight packing materials viz., hollow Poly Vinyl Chloride (PVC), solid cardboard and timber, were used as packing material in the compression zones of the beam specimens. All the three packing materials were selected based on their lightweight property, which will not defeat the key features of lightweight CFS construction, like and fastened to it using the same self-drilling screws. Three types of light-weight packing materials viz., hollow Poly Vinyl Chloride (PVC), solid cardboard and timber, were used as packing material in the compression zones of the beam specimens. All the three packing materials were selected based on their lightweight property, which will not defeat the key features of lightweight CFS construction, like concrete.

Table 1 Labelling of the specimens

Specimen	Labelling	Profile adopted	Packing in flange	Packing in web
1	BB	A	-	-
2	PF	A	Hollow PVC	-
3	CF	A	Cardboard	-
4	PFPW	B	Hollow PVC	Hollow PVC
5	CFPW	B	Cardboard	Hollow PVC
6	CFCW	B	Cardboard	Cardboard
7	TFTW	B	Timber	Timber

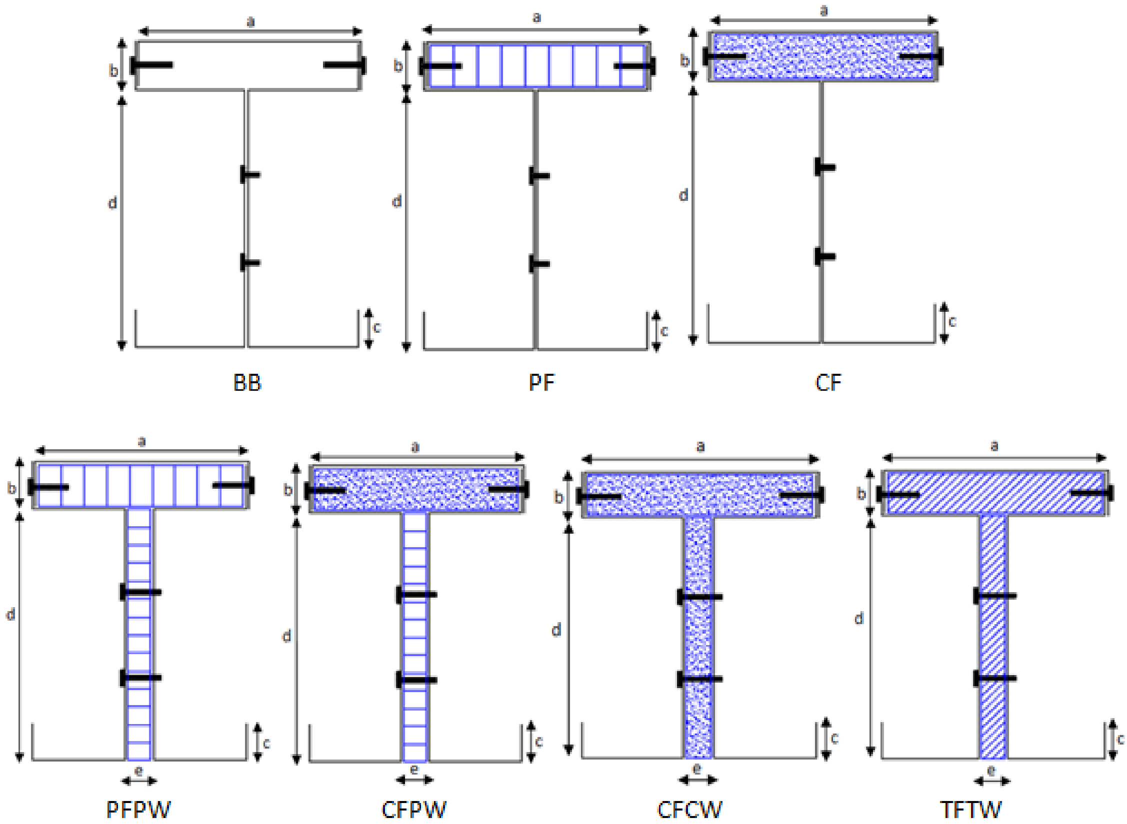

Fig. 3 Cross-sectional profiles of various specimens

Table 2 Nominal and measured dimensions of the specimens

Specimen	Weight Kg/m	Thickness (mm)	Nominal dimensions (mm)					Measured dimensions (mm)				
			a	b	c	d	e	a	b	c	d	e
BB	12.07	1.6	150	30	25	200	-	153	30	24	203	-
PF	13.02	1.6	150	30	25	200	-	152	32	26	203	-
CF	13.93	1.6	150	30	25	200	-	153	31	23	201	-
PFPW	13.23	1.6	150	30	25	200	25	151	32	25	204	26
CFPW	15.47	1.6	150	30	25	200	25	150	33	26	200	25
CFCW	17.76	1.6	150	30	25	200	25	154	30	23	202	23
TFTW	15.19	1.6	150	30	25	200	25	152	33	24	204	24

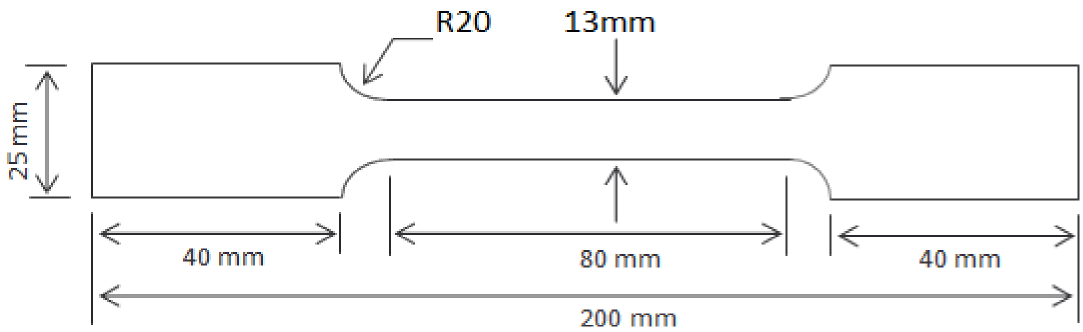

Fig. 4 Details of the tensile coupon specimen

Fig. 5 Tensile coupons before testing

The specimens were labeled based on the packing used in the flange and web, the details of which are given in Table 1. Fig. 2 shows the overall view of the test specimens before testing. Fig. 3 shows the cross-sectional details of various specimens. Table 2 gives the dimensional details of various specimens.

3. Material testing

To determine the accurate stress vs. strain relationship of tensile tests of steel coupons taken from different sheets were conducted. The coupons were cut along the longitudinal direction of the specimens. Tensile coupon dimensions were chosen in accordance with IS 1608-2005, as shown in Fig. 4. Five coupon specimens were prepared to complete the material testing, as shown in Fig. 5. A computerized after fabricating the various specimens. The bottom flange-to-web junction location was used to measure the geometric imperfections both in longitudinal as well as transverse directions. The readings at the mid-span of the test specimens were obtained by using an optical theodolite and a calibrated digital vernier caliper. The imperfections were measured at the mid-span of the specimens, along the two orthogonal Universal Testing Machine (UTM) of 100kN capacity was used to carry out the tensile tests of the coupons. All the required operations were performed automatically after the tensile specimen(coupon) was mounted in the jaws of the machine. The load and elongation parameters were carefully monitored using the inbuilt data acquisition system attached to a personal computer of the UTM. The typical stress vs. strain plot of coupon 4 is shown in Fig. 6. The average of the results of tensile tests is given in Table 3. The material properties for PVC, cardboard, and timber as obtained from the supplier are also given in Table 3.

Table 3 Material properties of the steel used

Material	$F_{compressive}$ (MPa)	E (GPa)	F_y (MPa)	F_u (MPa)	δ (%)
CFS	-	209	367.95	425.64	21
PVC	5	1.5	-	-	-
Cardboard	44	14	-	-	-
Timber	36	11	-	-	

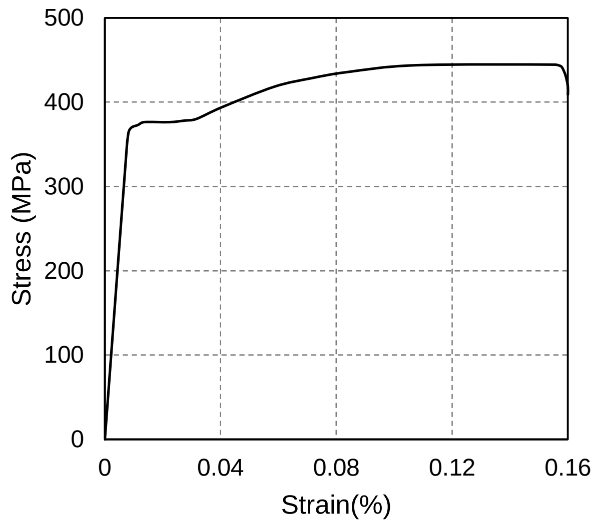

Fig. 6 Stress vs. strain curve of CFS used

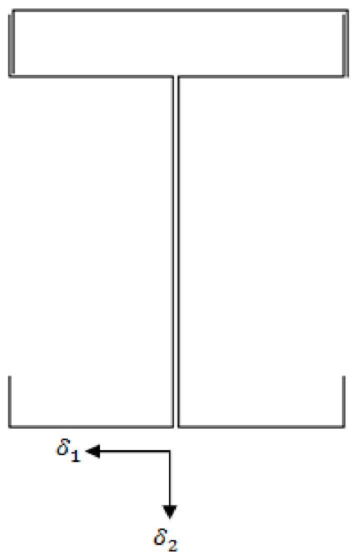

Fig. 7 Direction of imperfection measurement

Table 4 Geometric imperfections measured in the specimens

b	BB	PF	CF	PFPW	CFPW	CFCW	TFTW
δ_1/L	1/2215	1/1513	1/2361	1/1952	1/1859	1/2238	1/3526
δ_2/L	1/1859	1/1681	1/2658	1/1489	1/2249	1/3163	1/2630

4. Geometric imperfections

The initial geometric imperfections were noted, soon directions (Fig. 7), and are given in Table 4. Maximum geometric imperfection measured at mid-span in δ1 & δ2 directions were 1/1513 mm and 1/1489 mm, respectively and were found in specimen PF and PFPW respectively. The minimum imperfection observed for specimen TFTW and CFCW at mid-span was 1/3526, 1/3163 in δ1 & δ2 direction, respectively. For the sake of comparison, the magnitude of the maximum and minimum imperfections measured by Dar *et al.* (2018b) were 1/2167 and 1/4112 respectively.

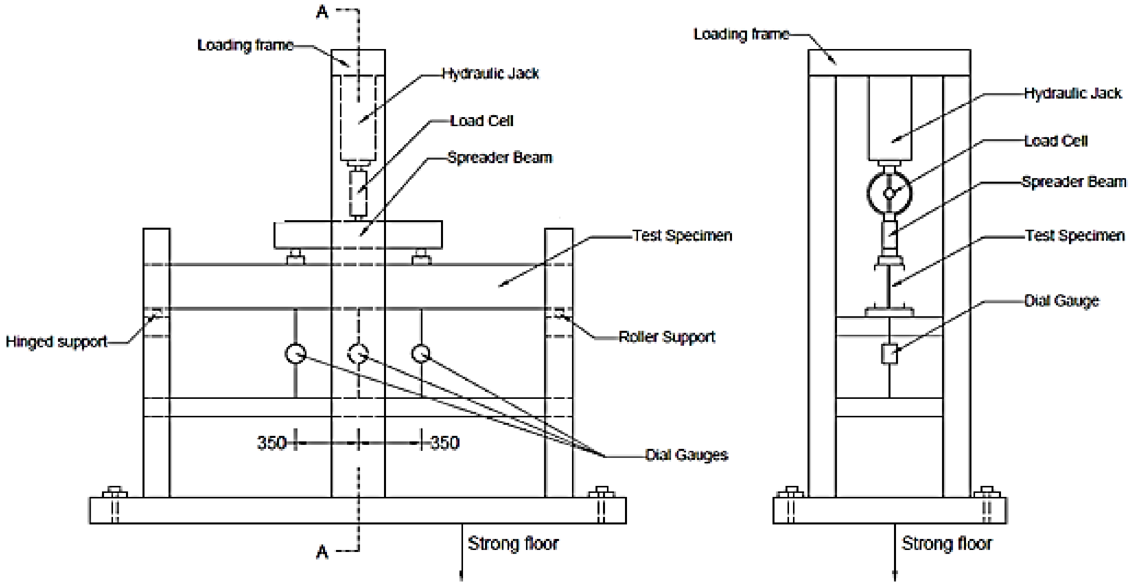

Fig. 8 Details of the test set-up

5. Test setup

The flexural tests were performed using a loading frame with a capacity of 500 kN as shown in Fig. 8. The specimens were loaded until failure, using a four-point flexural test set-up, to ensure uniform bending moment and zero shear force within the central region of the specimen. The schematic view of the test set-up is shown in Fig. 9. Simply supported end conditions were adopted for the beam specimens with a total span of 2300 mm and an effective span of 2100 mm. A heavy spreader beam(comprising of two hot-rolled channels ISMC 100×50welded toe-to-toe) was used to transfer the concentric loading applied by the manually operated hydraulic jack on to the specimen's two loading points. The loading points were at a distance of span/3 from the supports. A proving ring (Load cell) of 100kN capacity was mounted between the loading jack and the spreader beam to record the load being applied. Three digital dial gauges (with least count of 0.01 mm and range 0-50 mm) were mounted, two being at the loading points and one at the mid-span. The specimens were loaded at constant rate and the dial gauge readings were recorded at every increment of five divisions in the proving ring, until failure. During the tests, the load was recorded by a proving ring whereas the vertical mid-span displacements were measured using three digital dial gauges located at mid-span and loading points. To evaluate the performance of different packing materials towards improving the structural performance CFS beams, it was necessary that the various parameters like beam span, end-support conditions, location of applied point loads and bearing stiffener arrangement under point load/reaction points are kept the same (Dar *et al.* 2017, 2015b). The other details of the test set-up can be found elsewhere (Dar *et al*. 2017, 2019d).

6. Test results and discussions

The test results were primarily interpreted based on the peak loads resisted by the specimens, the flexural capacities developed by the same and their failure modes. The moment capacities were quantified as the product of the reaction force and the shear zone length (distance between the support reaction and the point of loading application on the specimen). The other details pertaining to this can be found in Dar *et al*. (2019b). Fig. 10 shows the load vs. mid-span displacement response of all the specimens. The BB specimen carried a maximum load of 50.36 kN with the corresponding mid-span displacement of 13.11 mm and developed a flexural resistance of 17.63 kNm. The specimen failure was initiated by local buckling of compression flange lip in the flexural zone at a load of around 19 kN, which progressed with the increase in loading, as shown in Fig. 11(a). This failure was accompanied by distortional buckling of the compression flange as shown in Fig. 11(b). The increase in loading led to the distortion of the bottom portion of the compression flange in between the screw locations, which is connected to the web. The screw spacing also affected this instability, as the screws hold the lower compression flange with the upper one. Noticeable distortion of the top rectangular flange was observed at a load of about 31 kN as shown in Fig. 11(b). Local failure of the bearing stiffener and punching failure in the compression flange was also observed (as shown in Fig. 11(c)).

The PF specimen carried a maximum load of 46.78 kN with the corresponding mid-span displacement of 6.59 mm and developed a flexural resistance of 16.37 kNm. In this specimen, the breakage of PVC box packing initiated the failure, under the loading points. The breakage sound was heard at a load of about 15 kN. Once the PVC packing failed, the local buckling of compression flange lip in the

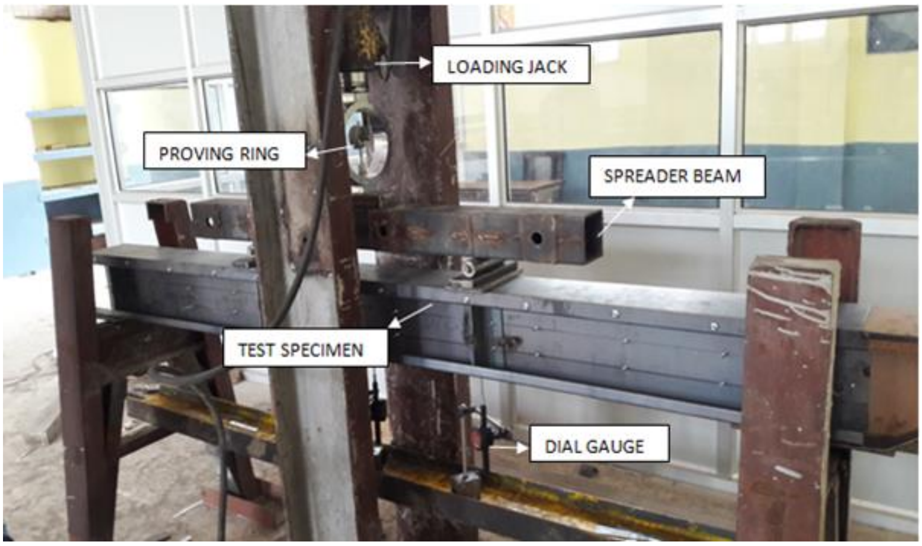

Fig. 9 Schematic view of the test set-up

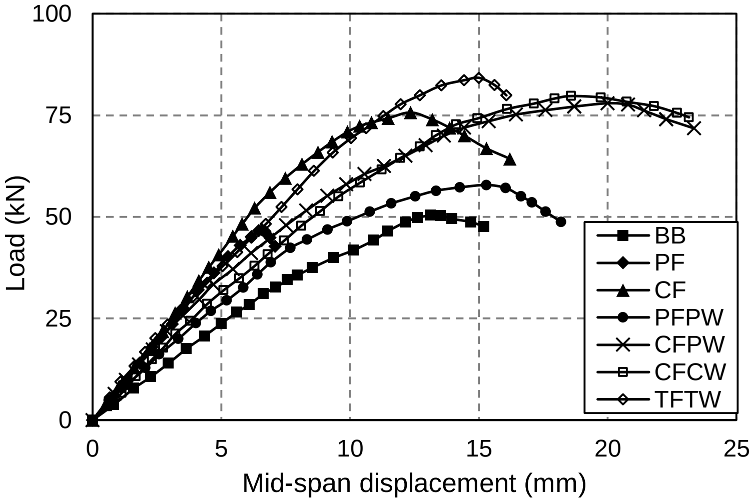

Fig. 10 Load vs. mid-span displacement response of the specimens

flexural zone was initiated as shown in Fig. 12(a) and observed at a load of around 27 kN. This lip buckling progressed with an increase in loading. Furthermore, compression flange buckling was also observed, as shown in Fig. 12(b). Like specimen BB, local failure of the bearing stiffener and punching failure in the compression flange was observed. This failure including its progression is shown in Fig. 12(c). With the increase in loading beyond 27 kN, the compression flange and edge stiffener started rotating about the flange-web junction leading to distortion of the rectangular flange as shown in Fig. 12(d).

The CF specimen carried a maximum load of 75.67 kN with the corresponding mid-span displacement of 12.35 mm and developed a flexural resistance of 26.48 kNm. Local buckling of the lip in the compression flange near both the loading points at around 57 kN load was observed as shown in Fig. 13(a). With the increase in loading, the specimen distorted progressively in between the screws, as the packing material was more influential in improving the local buckling resistance of the beam sections. Finally, a prominent distortion was observed at a load of about 75 kN as shown in Fig. 13(b).

The PFPW specimen carried a maximum load of 57.82 kN with the corresponding mid-span displacement of 15.29 mm and developed a flexural resistance of 20.23 kNm. The Specimen failed by the combination of local compression lip buckling, distortional buckling, web buckling and bearing failure at the supports. The sound of PVC breakage was heard at a load of around 29 kN. This was followed by the local buckling of the lip of compression flange at a load of around 44 kN. Fig. 14(a) shows compression lip buckling and bearing failure of the specimen. In the last stage of loading, web buckling was observed at a load of 56 kN, leading to minor distortion (see Fig. 14(b)).

(a) Local bucking in the lip of rectangular compression flange

(b) Distortion of the compression flange

(c) Local failure of the bearing stiffener and punching failure in the compression flange

Fig. 11 Failure modes in specimen BB

The PFCW specimen carried a maximum load of 78.01 kN with the corresponding mid-span displacement of 19.99 mm and developed a flexural resistance of 27.30 kNm. The failure of this specimen started by local buckling of compression flange lip near both the loading points at a load of about 61 kN as shown in Fig. 15(a). This failure was later accompanied by bearing failure at the loading points as shown in Fig. 15(a). The web of the specimen also showed signs of buckling, leading to distortion, as shown in Fig. 15(b). In this case, since there was good integrity between the cardboard packing and the compression flange, the buckling stability of the compression flange improved significantly. The relative difference between the stiffness of the flange and the web due to the incorporation of cardboard in the flange and PVC in the web region led to this type of distortional behaviour. Finally, with the increase in loading, the mid-span displacement increased significantly.

The CFCW specimen carried a maximum load of 79.76 kN with the corresponding mid-span displacement of 18.59 mm and developed a flexural resistance of 27.91 kNm. During the entire loading process, no remarkable instability

(b) Local bucking in the lip of rectangular compression flange

(a) Local bucking in the rectangular compression flange

(c) Local failure of the bearing stiffener and punching failure in the compression flange

(d) Distortion of the compression flange

Fig. 12 Failure modes in specimen PF

failure occurred anywhere in the specimen, except a little elastic buckling of compression flange lip at a load of about 69 kN in the flexural zone as shown in Fig. 16(a). Upon unloading, this elastic buckling instability was reversed as shown in Fig. 16(b). When the loading was increased beyond 69kN the vertical mid-span displacement increased and the specimen failed by flexural failure as shown in Fig. 16(c).

The TFTW specimen carried a maximum load of 84.22 kN with the corresponding mid-span displacement of 15.01 mm and developed a flexural resistance of 29.71 kNm.

The failure of this specimen was initiated by local buckling of the compression flange lips near both the loading points at a load of 70kN as shown in Fig. 17. Upon further loading, no remarkable secondary failure was observed, except for minor bearing failure, primarily due to concentrated loading.

The summary of results, the design strengths predicted by North American Specifications for cold-formed steel structures (AISI S-100) and Indian Standards for cold-formed steel structures (IS 801) are presented in Table 5.

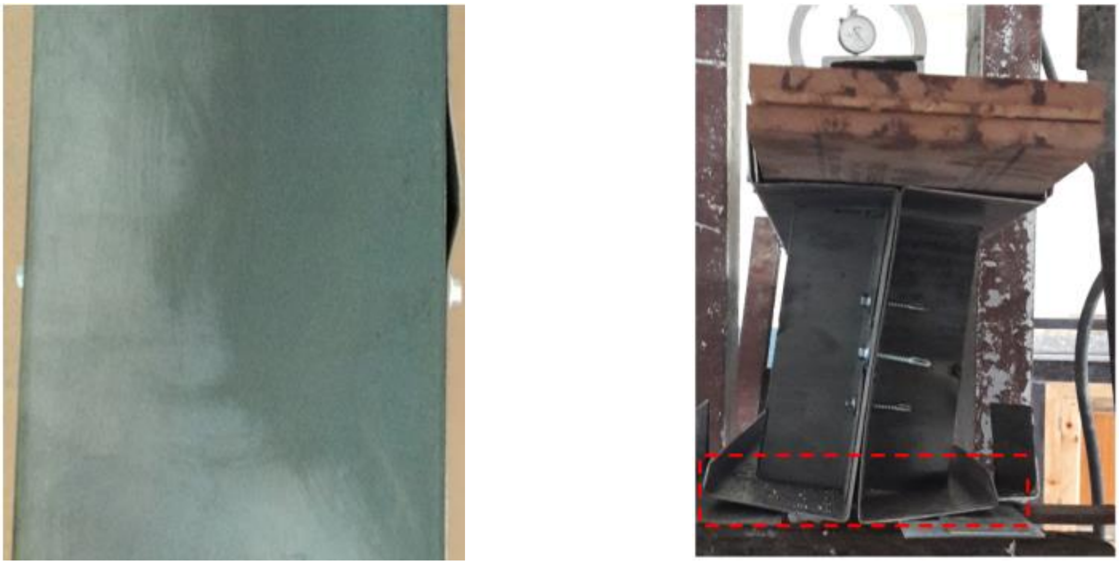

(a) Minor local bucking in the lip of rectangular compression flange (b) Prominent distortional buckling observed

Fig. 13 Failure modes in specimen CF

(a) Local buckling of lip in compression zone and bearing failure at the loading point

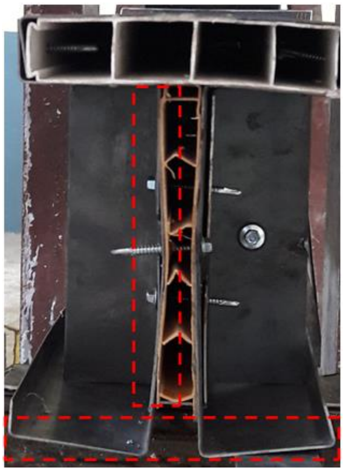

(b) Web buckling and minor distortion

Fig. 14 Failure modes in specimen PFPW

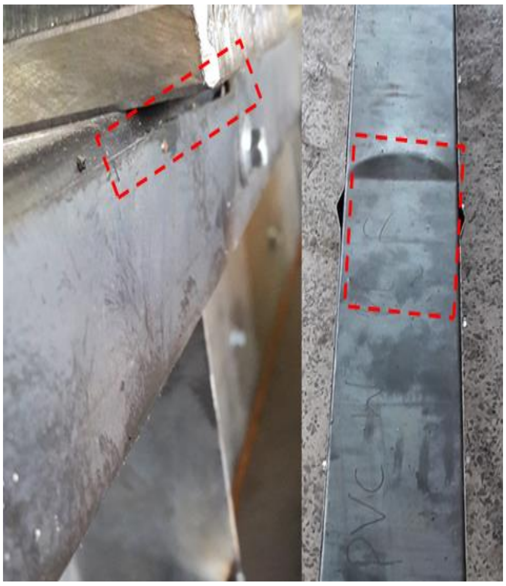

(a) Local buckling of lip in compression zone and flange buckling at the loading point

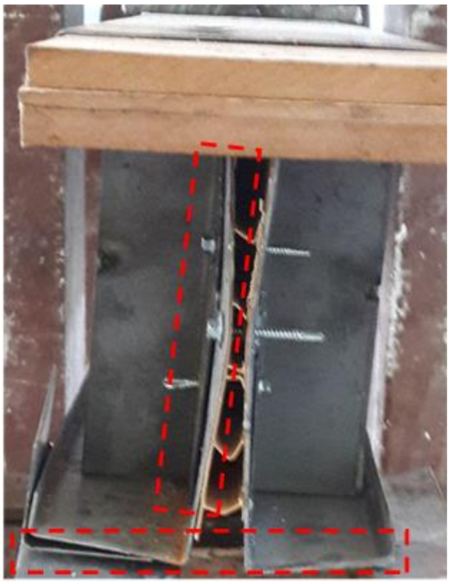

(b) Web buckling and distortion

Fig. 15 Failure modes in specimen PFCW

(a) Elastic local buckling of lip in compression

(b) Reversal of elastic local buckling of lip in compression after unloading

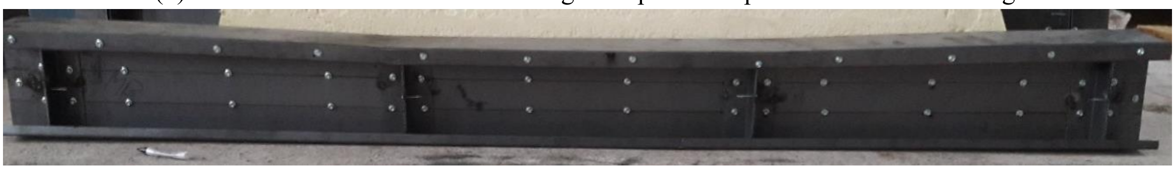

(c) Flexural buckling failure

Fig. 16 Failure modes in specimen CFCW

Table 5 Summary of results

Specimen	P_{NAS} (kN)	P_{IS} (kN)	P_{Exp} (kN)	M_{Exp} (kNm)	M_y (kNm)	M_p (kNm)	M_{Exp}/M_y	M_{Exp}/M_p	k (kN/mm)	Failure modes
BB			50.36	17.63			0.89	0.66	4.66	LB + DB + BF
PF	56.32	54.83	46.78	16.37	19.71	26.71	0.83	0.61	7.38	LB + FB + DB + BF
CF			75.67	26.48			1.34	0.99	8.29	LB + DB
PFPW			57.82	20.23			1.03	0.8	5.6	LB + WB + DB + BF
CFPW			78.01	27.3			1.39	1.07	6.52	LB + FB + WB + DB
CFCW	56.15	52.51	79.76	27.91	19.65	25.35	1.42	1.1	6.03	$F_{lxr}B$
TFTW			84.22	29.47			1.5	1.16	7.52	LB + BF

Fig. 17 Local buckling of lip of the compression flange

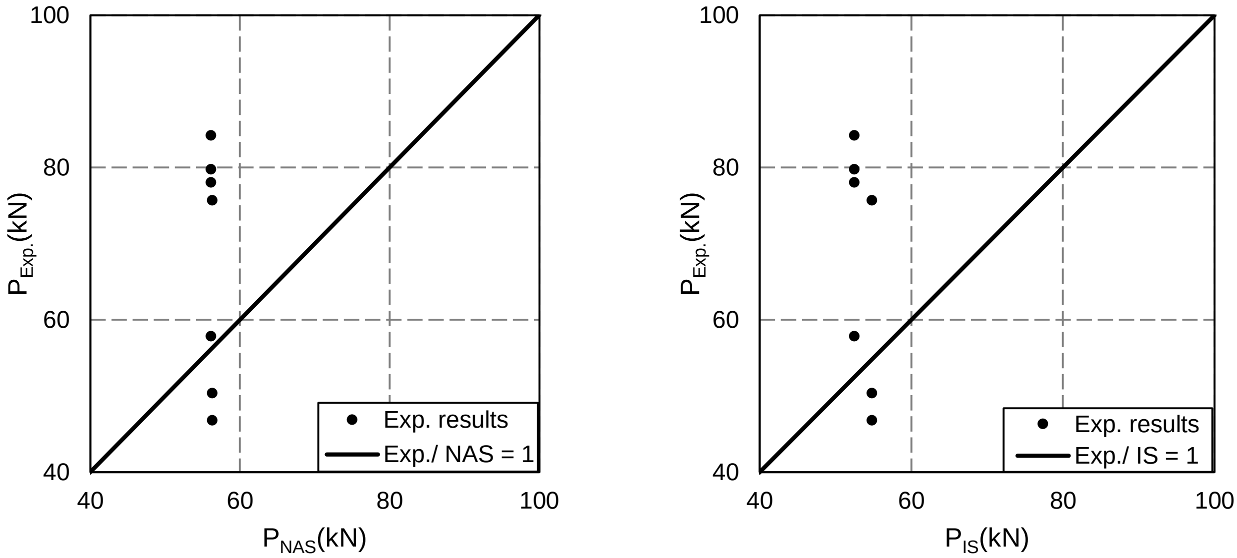

Fig. 18 Comparison of experimental results with the design strengths

The comparison of the design strengths with the experimental results are shown in Fig. 18. The design strength of the CFS portion only was quantified by using both the standards. No interaction between the CFS portion and the packing material was assumed for the quantification of the design standards. The ultimate capacity of the CFS section remarkably improved by adopting hard cardboard and timber as packing, particularly in the flange region. The interaction between CFS and these packing materials enhanced the flexural capacity of these sections. Specimens with profile A performed better than the ones with profile B, as the rectangular web displayed better stability. With more ductility, the post-peak behaviour of CFPW and CFCW specimens was slightly better than that of the other specimens. The flexural strength, stiffness and strength/weight comparison of various specimens are shown

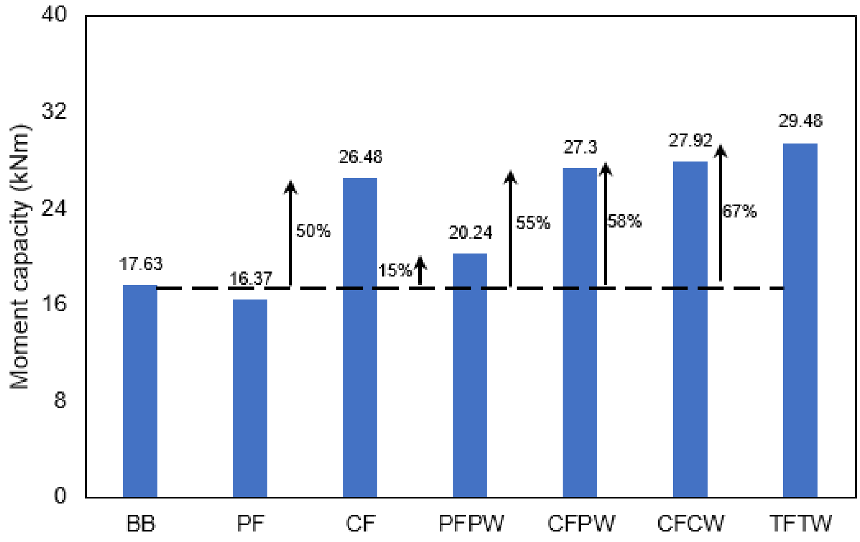

Fig. 19 Flexural strength comparison of various specimens

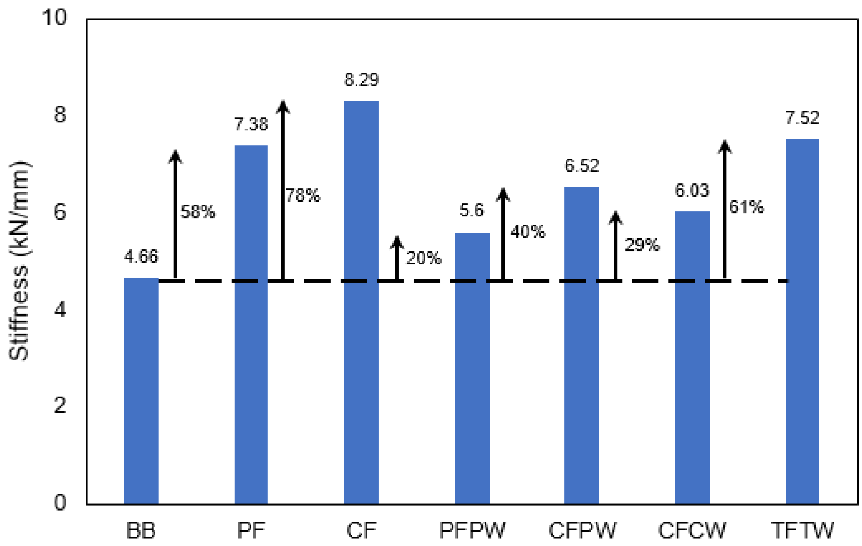

Fig. 20 Stiffness comparison of various specimens

in Figs. 19-21 respectively. The arrows indicate the percentage enhancement if the various performance levels, as shown in Figs. 19-21. The TFTW specimen performed the best with reference to flexural strength consideration (around 67%). The cardboard packing in the web for CFCW did not contribute much towards the flexural strength enhancement (mere 3%) compared to the PVC packing in the web for CFPW. However, the use of cardboard as packing in the flange of CFPW lead to a 40% improvement in the flexural strength, when compared to the PFPW specimen. It was also seen that for sections with profile A, the cardboard packing in the flange (CF specimen) improved the flexural strength significantly, by around 50%. The drop in the flexural strength of PF specimen attributed to the larger geometric imperfections when compared to BB specimen. The CF specimen performed the best with reference to stiffness consideration. This was primarily due to the double thickness of the web. It is worth noting that the PF specimen performed satisfactorily in terms of stiffness consideration, mainly due to PVC packing in the flange, which provided the additional stiffness until the PVC failed by strength failure. However, the same PVC packing could not perform satisfactorily in PFPW specimen, as the web failed by stability failure leading to distortion. By delaying the local buckling instabilities, the cardboard and timber packing improved the flexural capacity of the specimens beyond their plastic moment capacities, which indicates that the composite action between the CFS and these two packing materials have immense potential to carry higher loads. Hence, such packing is recommended for composite cold form sections with rectangular top flange.

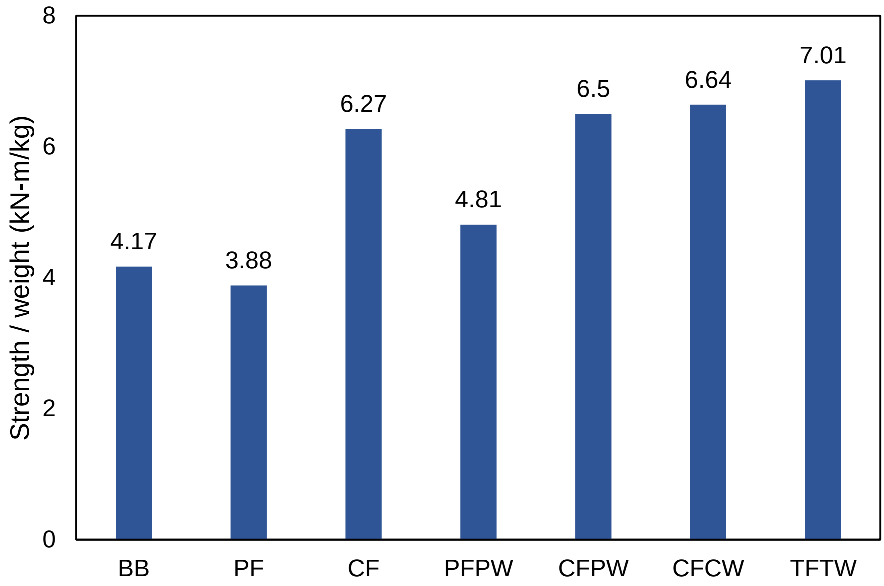

Fig. 21 Strength/weight comparison of various specimens

5. Conclusions

The behavior of rectangular compression flanged CFS composite beams was investigated experimentally with different packing materials. Four-point flexural tests were carried out on seven specimens to assess the flexural capacity, failure modes and deformed shapes of the CFS composite beam. Based on the experimental investigations, the following conclusions are drawn.

- The novel rectangular compression flanged CFS composite beams, with innovative packing materials, performed well in terms of strength and stiffness characteristics. The ultimate capacity of the section remarkably improved by adopting hard cardboard and timber as packing, particularly in the flange region. The interaction between CFS and these packing materials enhanced the flexural capacity of these sections. Hence, the objectives of this study were successfully fulfilled.
- Local buckling of the compression flange, bearing failure near the supports, web buckling, local buckling in the bearing stiffener, and distortional buckling were the types of failures observed.
- For the group of sections with profile A, the performance enhancement in CF specimen was significant, as the cardboard packing in the flange improved the flexural strength drastically, by around 50%. For the group of sections with profile B, the performance of TFTW specimen was the best from flexural strength consideration. The cardboard packing in the web of CFCW did not help much towards the flexural strength enhancement (mere 3%), when compared to the PVC packing in the web for CFPW. However, the introduction of cardboard packing in the flange of CFPW lead to a 40% improvement in the flexural strength, when compared to the PFPW specimen. The presence of PVC packing in the web could not eliminate the web buckling in PFPW and CFPW specimens.
- From stiffness consideration, the CF specimen performed the best, which was primarily due to the double thickness of the web. The stiffness performance of the PF specimen was satisfactory, which was mainly due to PVC packing in the flange, which provided the additional stiffness until the PVC failed by strength failure. However, the same PVC packing could not perform satisfactorily in PFPW specimen, as the web failed by stability leading to distortion.
- The cardboard and timber packing improved the strength of the specimens that further improved the strength/weight ratio of the specimens, thus making such CFS composite section highly efficient. Furthermore, hard cardboard is an environment-friendly material and has immense potential to delay or even eliminate buckling instabilities, especially in the flange region.
- The PVC packing in the flange failed to prevent the punching failure due to the bearing stiffener at the loading points. However, such a failure was not observed near the supports. Further, the PVC packing delayed the initiation of buckling failure in PF and PFPW specimens marginally, but could not avoid other failure modes. Bearing stiffener of higher thickness could have prevented/delayed the punching type of failure.
- Local buckling of the compression flange lip initiated from the loading points and later covered the entire pure moment zone. This type of buckling primarily occurred in BB, PF and PFPW specimens. However local buckling was not predominant in other specimens, due to higher stiffness provided by packing like cardboard and timber in the flange region.
- The cardboard packing in the compression flange of CFCW prevented bearing failure and flange distortion, due to better stability of the cross-section. The buckling of the web was completely eliminated in CFCW and

TFTW specimens. Thus, rendering hard cardboard and timber as materials that possess sufficient capability to utilize the full capacity of the web. The flange distortion was completely eliminated in CF, CFPW, CFCW and TFTW specimens. Hence, both timber and hard cardboard are recommended in such CFS composite beams with rectangular compression flange.

Given the performance studies on the various CFS composite beams, the authors recommend the use of CFS sections with profile B, which has better resistance against the various instabilities encountered in CFS sections with profile A. Furthermore, the same packing material should be used in both the flange as well as the web to prevent the formation of relative stiffness between the two, which can lead to distortional buckling instabilities. The use of PVC should be avoided as it could not assist the CFS beams in developing sufficient local buckling resistance that could improve the overall flexural performance in those CFS composite beams.

References

Awaludin, A., Rachmawati, K., Aryati, M. and Danastri, A.D. (2015), "Development of cold formed steel-timber composite for roof structures: compression members", *Procedia Eng.*, **125**, 850-856. https://doi.org/10.1016/j.proeng.2015.11.052.

Biggs, K.A., Ramseyer, C., Ree, S. and Kang, T.H. (2015), "Experimental testing of cold-formed built-up members in pure compression", *Steel Compos. Struct.*, **18(**6), 1331-1351. https://doi.org/10.12989/scs.2015.18.6.1331.

Dar, M.A., Subramanian, N., Dar, A.R., Lim, Anbarasu, M., J.B.P., and Mir, A. (2019a), "Behaviour of partly stiffened cold-formed steel built-up beams: Experimental investigation and numerical validation", *Adv. Struct. Eng.*, **22**(1) 172-186. https://doi.org/10.1177/1369433218782767.

Dar, M.A., Subramanian, N., Dar, A.R., Majid, M., Haseeb, M. and Tahoor, M. (2019b), "Structural efficiency of various strengthening schemes for cold-formed steel beams: Effect of global imperfections", *Steel Compos. Struct.*, **30**(4), 393-403 https://doi.org/ 10.12989/scs.2019.30.4.393.

Dar, M.A., Subramanian, N., Rather, A.I., Dar, A., Lim JBP, Anbarasu M. and Roy, K. (2019c), "Effect of angle stiffeners on the flexural strength and stiffness of cold-formed steel beams", *Steel Compos. Struct.*, **33**(2), 225-243. https://doi.org/ 10.12989/scs.2019.33.2.225.

Dar, M.A., Subramanian, N., Dar, A.R., Rather, A.I., Mir, A. and Syed, S., (2019d), "Strengthening of capacity deficient RC beams- An experimental approach", *Struct. Eng. Mech.*, **70**(3), 303-310. https://doi.org/ 10.12989/sem.2019.70.3.303.

Dar, M.A., Sahoo, D.R., Pulikkal, S. and Jain, A.K. (2018a), "Behavior of laced built-up cold-formed steel columns: Experimental investigation and numerical validation", *Thin Wall. Struct.*, **132**, 398-409. https://doi.org/10.1016/j.tws.2018.09.012.

Dar, M.A., Subramanian, N., Dar, A.R., Anbarasu, M. and Lim, J.B.P. (2018b), "Structural Performance of Cold-formed Steel Composite Beams", *Steel Compos. Struct.*, **27**(5), 545-554. https://doi.org/ 10.12989/scs.2018.27.5.545.

Dar, M.A., Subramanian, N., Dar, A.R. and Raju, J. (2017), "Rehabilitation of a distressed steel roof truss – A study", *Struct. Eng. Mech.*, **62**(5), 567-576. https://doi.org/ 10.12989/sem.2017.62.5.567.

Dar, M.A., Dar, A.R., Yusuf, M. and Raju, J. (2015a), "Experimental study on innovative sections for cold formed steel beams", *Steel Compos. Struct.*, **19**(6), 1599-1610. https://doi.org/10.12989/scs.2015.19.6.1599.

Dar, M.A., Subramanian, N., Dar, A.R. and Raju, J. (2015b), "Experimental investigations on the structural behaviour of a distressed bridge", *Struct. Eng. Mech.*, **56**(4), 695-705 https://doi.org/ 10.12989/sem.2015.56.4.695.

Gao, F., Zhu, H.P., Zhang, D.H. and Fang, T.S. (2014), "Experimental investigation on flexural behavior of concrete-filled pentagonal flange beam under concentrated loading", *Thin Wall. Struct.*, **84**, 215-225. https://doi.org/10.1016/j.tws.2014.06.008.

Hancock, G.J. (2016), "Cold-formed steel structures: Research review 2013–2014", *Adv, Struct. Eng.*, **19**(3), 1-16. https://doi.org/10.1177/1369433216630145.

Hassanein, M.F. (2015), "Fundamental behavior of concrete-filled pentagonal flange plate girders under shear", *Thin Wall. Struct.*, **95**, 221-230. https://doi.org/10.1016/j.tws.2015.07.003.

Hassanein, M.F., Kharoob, O.F. and Taman, M.H. (2017) "Experimental investigstion of cementicious material-filled square thin-walled steel beams", *Thin Wall. Struct.*, **114**, 134-143. https://doi.org/10.1016/j.tws.2017.01.031.

IS 801(1975), *Code of Practice for Use of Cold Formed Light Gauge Steel Structural Members in General Building Construction*, Bureau of Indian Standards, New Delhi, India.

Javed, M.F., Hafizah, N., Memon, S.A., Jameel, M. and Aslam, M. (2017), "Recent research on cold-formed steel beams and columns subjected to elevated temperature: A review", *Constr. Build. Mater.*, **144**, 686-701. https://doi.org/10.1016/j.conbuildmat.2017.03.226.

Khate, K., Patton, M.L. and Marthong, C. (2018) "Structural behaviour of stainless steel stub column under axial compression: a FE study", *Int. J. Steel Struct.*, **18**, 1-18. https://doi.org/10.1007/s13296-018-0083-1.

Kim, S., Yom, K. and Choi, S. (2015), "A study on the structural performance of new shape built-up square column under concentric axial load", *Steel Compos. Struct.*, **18(**6), 1451-1464. https://doi.org/ 10.3850/978-981-07-2615-7_237.

Kumar, N. and Sahoo, D.R. (2016), "Optimization of lip length and aspect ratio of thin channel sections under minor axes bending", *Thin-Wall. Struct.*, **100**, 158-169. https://doi.org/10.1016/j.tws.2015.12.015.

Li, Y., Shan, W., Shen, H., Zhang, Z. and Liu, J. (2014), "Bending resistance of I-section bamboo-steel composite beams utilizing adhesive bonding", *Thin Wall. Struct.*, **89**, 17-24. https://doi.org/10.1016/j.tws.2014.12.007.

Magnucka-Blandzi, E. (2010), "Effective shaping of cold-formed thin-walled channel beams with double-box flanges in pure bending", *Thin Wall. Struct.*, **49**(1), 121-128. https://doi.org/10.1016/j.tws.2010.08.013.

Muftah, F., Sani, M.S.H.M. and Kamal, M.M.M. (2019), "Flexural strength behaviour of bolted built-up cold-formed steel beam with outstand and extended stiffener", *Int. J. Steel Struc.*, **19**(3), 719-732. https://doi.org/10.1007/s13296-018-0157-0.

Priyanga, R.S. and Ramalingam, R. (2018), "In plane compression behaviour of steel profle sheets", *Int. J. Steel Struct.*, **19**(1), 293-300. https://doi.org/10.1007/s13296-018-0116-9.

Sani, M.S.H.M., Kamal, M.M.M, Muftah, F. and Tan, C.S. (2016), "Flexural performance of built-up cold-formed steel beam filled with compacted soil", *J. Eng. Appl. Sci.*, **11**(16), 9855-9862.

Sani, M.S.H.M., Muftah, F. and Ismail, M.I. (2018), "Testing and analysis of cold-formed steel channel section with notch", *Int. J. GEOMATE*, **14**(43), 42-49. https://doi.org/10.21660/2018.43.3539.

Sani, M.S.H.M., Muftah, F. and Osman, A.R. (2019), "A review and development of cold-formed steel channel columns with oriented strand board sections", *Mater. Today Proceedings*, **17**(3), 1078-1085 https://doi.org/10.1016/j.matpr.2019.06.519.

Sharafi, P., Mortazavi, M., Usefi, N., Kildashti, K., Ronagh, H. and Samali, B. (2018), "Lateral force resisting systems in lightweight steel frames: Recent research advances", *Thin Wall. Struct.*, **130**, 231-253. https://doi.org/10.1016/j.tws.2018.04.019.

Siahaan, R., Keerthan, P. and Mahendren, M. (2018), "Section moment capacity design rules for rivet fastened rectangular hollow flange channel beams", *Thin Wall. Struct.*, **127**, 781-797. https://doi.org/10.1016/j.tws.2018.02.013.

Usefi, N., Sharafi, P. and Ronagh, H. (2019), "Numerical models for lateral behaviour analysis of cold-formed steel framed walls: State of the art, evaluation and challenges", *Thin Wall. Struct.*, **138**, 252-285. https://doi.org/10.1016/j.tws.2019.02.019.

Valsa Ipe, T., Sharada Bai, H., Manjulavani, K. and Merchant Mohd Zafar Iqbal (2013) "Flexural behaviour of cold-formed steel-concrete composite beams" *Steel Compos. Struct.*, **14**(2), 105-120. https://doi.org/10.12989/scs.2013.14.2.105.

Yang, Y. and Lui, E.M. (2012), "Behavior and design of steel I-beams with inclined stiffeners", *Steel Compos. Struct*., **12(**3), 183-205. https://doi.org/10.12989/scs.2012.12.3.183.

Ye, J., Hajirasouliha, I., Becque, J. and Pilakotus, K. (2016) "Development of more efficient cold formed steel channel sections in bending", *Thin Wall. Struct.*, **101**, 1-13. https://doi.org/10.1016/j.tws.2015.12.021.

CC

Notations

BB	: Benchmark beam.
BF	: Bearing failure.
CF	: Beam with hard cardboard in flange.
CFCW	: Beam with hard cardboard in both flange and web.
CFPFB	: Concrete Filled Pentagonal Flange Beam.
CFPW	: Beam with hard cardboard in flange and hollow PVC in web.
CFS	: Cold-formed steel.
DB	: Distortion buckling.
FB	: Flange buckling.
$F_{lxr}B$	: Flexural buckling.
HPFB	: Hollow Pentagonal Flange Beam.
LB	: Lip buckling.
M	: Moment carrying capacity of the specimen.
P_{IS}	: Design strength according to AS/NZS.
P_{EXP}	: Experimental failure load.
P_{NAS}	: Design strength according to AISI S-100.
PF	: Beam with hollow PVC in flange.
PFPW	: Beam with hollow PVC in both flange and web.
RHFCB	: Rectangular Hollow Flange Channel Beam.
TFTW	: Beam with timber in both flange and web.
W	: Weight per metre run of specimen in kgs.
WB	: Web buckling.
δ	: Mid-span displacement in mm.
$F_{compressive}$	: Compressive force resisted
E	: Young’s Modulus
F_y	: Yield strength
F_u	: Ultimate strength
δ (%)	: Percentage elongation in the tensile coupon.